Particle emission associated with deep inelastic α-particle scattering at 35 MeV/nucleon

H. Machner, U. Bechstedt, A. Budzanowski,* P. Jahn, and C. Mayer-Böricke
Institut für Kernphysik, Kernforschungsanlage Jülich, D-5170 Jülich, Federal Republic of Germany
(Received 5 March 1985)

Deep inelastically scattered α particles on ^{58}Ni have been measured with coincident protons and α particles in the reaction plane at $E_\alpha = 140$ MeV. The low energy proton spectra show evaporation-like patterns with angle dependent slope parameters. The coincident α-particle spectra could be measured up to higher energies than for protons. They show up contributions from knockout reactions. All data are in accordance with the assumption of statistical independence of the emission process and the four-momentum transfer. The preequilibrium region of the proton yield is well described by the exciton coalescence model.

I. INTRODUCTION

When an energetic projectile impinges on a target nucleus, fast secondary particles will most probably emerge. For the description of this fast particle emission many models—quantum mechanical as well as semiclassical—have been developed. A recent review is given in Ref. 1 for models treating the nuclear reaction as a series of two-body collisions. However, other models with very different physics are available such as the Fermi jet,[2,3] the hot spot,[4] and the moving source description[5] to account for the phenomenon of fast particle emission. Most of these models deal with only inclusive data first because a part of the models is tailored to such data, and second more exclusive data are scarce. It is, therefore, the aim of the present work to produce such data and hopefully discriminate between different model formulations.

For that purpose we have chosen the reaction ^{58}Ni$(\alpha,\alpha' c)$, with c a charged particle. Since an incident α particle has, at velocities close to the Fermi velocity, a rather small mean free path,[6] it seemed especially useful to test a subset of the models. A second advantage is the nonexistence of excited states below the breakup threshold in the α particle. Thus fluctuation effects as being reported by Schmitt *et al.* (Ref. 7) for heavier projectiles can be excluded. Furthermore, by proper selection of the α-scattering angle, one can avoid contributions from pickup to ^{5}Li followed by the breakup $^5\text{Li} \rightarrow \alpha + \text{p}$.[8,9] The possible focusing effects on the secondary charged particle by the deep inelastic scattered projectile is for α particles negligibly small, in contrast to heavy ion reactions.[10]

As a target nucleus ^{58}Ni was chosen because it is heavy enough not to be disturbed in the continuum due to level density effects by a special nuclear structure nor is its Coulomb barrier so high that the emission of low energy particles would be strongly suppressed.

First results of the present investigation have been published already in a Rapid Communication.[11] The paper is arranged as follows. In the next section details of the experiments are given. In Sec. III we discuss the experimental findings. Then the data are compared against various model predictions and our conclusions follow.

II. EXPERIMENTS

The experiments were carried out at the Jülich isochronous cyclotron JULIC. The α beam was focused with the aid of a pair of quadrupole magnets to the center of a scattering chamber 1 m in diameter. The beam was then refocused by another magnetic quadrupole lens to a Faraday cup which served as beam dump. A 99.8% isotopically pure ^{58}Ni target of 4.2 mg thickness was used. The inelastic scattered α particles were detected by a solid

TABLE I. Setup of the telescopes and their energy ranges. The lower energy limits were not determined by the indicated ΔE-counter thicknesses but by thresholds in the electronic circuits, and thus may be up to 20% larger.

	Telescope		
	α'	c_1	c_2
E_1 or $\Delta E_{\alpha'}$ (μm)	1000	50	50
E_2 (μm)		400	400
E_3 or $E_{\alpha'}$ (mm)	28 [Ge(Li)]	2×2.0	2.0
Solid angle (msr)	3.58	7.81	7.52
Opening angle	2.33°	5.7°	5.6°
Proton energy range (MeV)	~12–115	~2–28	~2–20
α-energy range (MeV)	~47–450	~8–105	~8–78

state telescope (denoted by α') consisting of a Si-surface barrier counter as ΔE counter and a Ge diode as E counter. Coincident charged particles were detected in two threefold Si-surface barrier telescopes (denoted by c_1 and c_2). Details of the telescopes are given in Table I. The α' telescope was placed at the angle $\vartheta_{\alpha'} = -30°$ with respect to the beam axis, and the two decay telescopes c_1 and c_2 were mounted in the reaction plane defined by the beam and the scattered α particles on a rotatable plate face to face to each other. The silicon counters were cooled to $-25°$C and the Ge counter to liquid nitrogen temperature. A sketch of the setup is given in Fig. 1.

Since the data acquisition system ND6660 used in the experiments allows the registration of only up to eight parameters, the following procedure was employed. The detector signals were amplified and the sum of the E_j counters, i.e., $\sum E_{1c_1,c_2}$, $\sum E_{2c_1,c_2}$, and $\sum E_{3c_1,c_2}$ and their total sums $\sum E_{c_1,c_2}$ recorded event by event on tape in list mode together with the total energy of the α' telescope and an output of an analog particle identification circuit. The time signal from an event in one of the detectors in the c telescopes and one in the α' telescope was fed into an additional analog-to-digital converter (ADC). The eighth signal recorded was a bit pattern which allowed a unique identification of the event. A more complete description of the experimental technique is given in Ref. 12.

Particle identification for the decay telescopes $c_{1,2}$ was performed later in an off-line analysis by gating signals with regions in the corresponding E_1-E_3 or E_2-E_3 maps and the corresponding bit in the eighth parameter. Chance coincidences were measured at a rate of less than 10% compared to real coincidences and were subtracted from the corresponding peak in the time spectrum.

The dead time of the setup including the ND6660 data acquisition system was measured by feeding signals into the preamplifiers from a pulse generator which was triggered by the down-scaled counting rate of the elastic scattered α particles, and the beam charge was corrected correspondingly. Because of the poor statistics, counting rate errors were between 5% and 100%. The systematic errors were estimated to be 15% in target thickness and uniformity, solid angle 1.3%, charge measurement $\leq 2\%$, and energy calibration $\leq 5\%$.

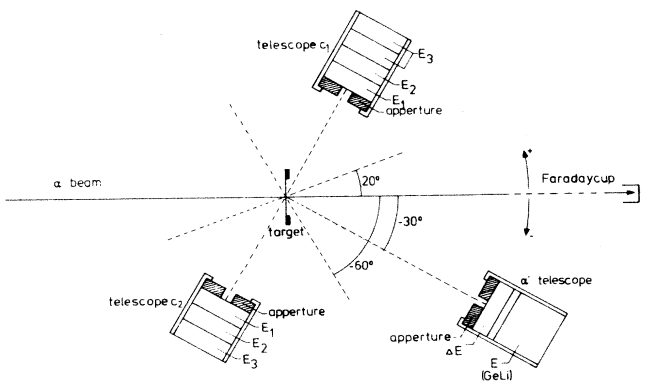

FIG. 1. Sketch of the experimental setup. Indicated also are the limitations in the detection angle ranges due to the geometry. The E_3 counter in the telescope c_1 is a stack of two 2 mm detectors.

III. EXPERIMENTAL RESULTS

Practically, only protons and α particles could be measured in coincidence with deep inelastically scattered α particles. To improve the counting rate statistics, data from the c telescopes were averaged over 1 MeV wide bins. The continuum of the α' spectrum from 55.5 MeV, which is well above the measuring threshold up to the threshold for proton decay, was divided into four bins each 19 MeV wide. Since the bin which corresponds to the smallest energy transfer may be strongly influenced by the decay properties of giant resonances, we will concentrate in the following on more inelastic events with mean energies $\bar{E}_{\alpha'} = 65$, 84, and 103 MeV. Proton spectra taken at different angles in the reaction plane in coincidence with α particles of energy $\bar{E}_{\alpha'} = 65$ MeV are shown in Fig. 2. The spectra show a maximum close to the Coulomb barrier and an exponential slope to higher energies. Only the most forward angle spectra show a more flat shape at energies above 15 MeV. The exponential shape reminds one of evaporation spectra.

In principle α'-p events could emerge from ^{5}Li decay. However, for the detection angle $\vartheta_{\alpha'} = -30°$ the ^{5}Li must have been in an excited state above 16 MeV, which is rather unlikely. Quasifree or knockout processes can be excluded, because the expected proton energies for such processes are outside the detection limits of the c telescopes, if serious distortions in the incoming and outgoing

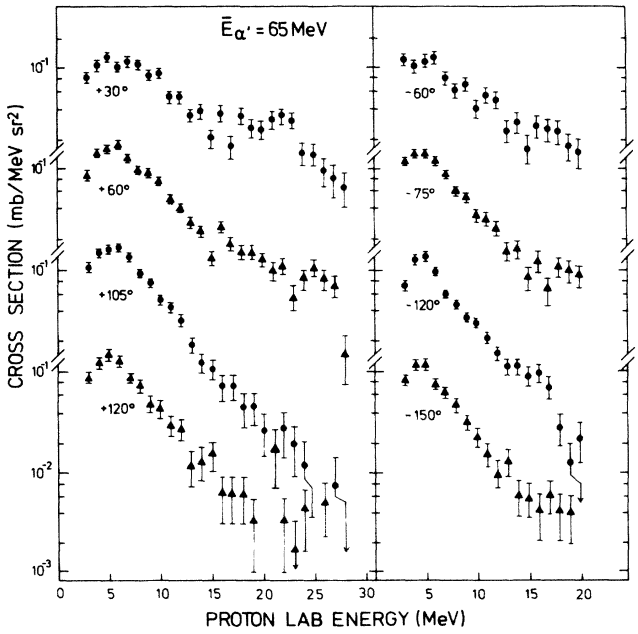

FIG. 2. Proton cross sections measured in coincidence with α' particles of energies (65±9.5) MeV. The proton detection angles are indicated in the figure.

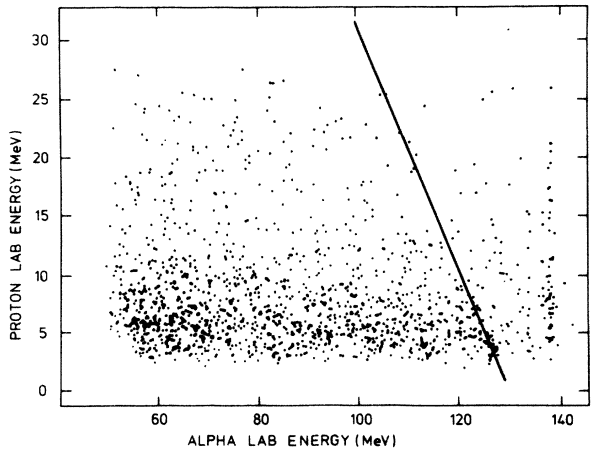

FIG. 3. Scatter plot for α'-p coincidences for a coplanar geometry $\theta_p = +30°$ and $\vartheta_{\alpha'} = -30°$. The kinematical loci for α'-p_0 events are shown as a solid curve. Chance coincidences with elastically scattered α particles are clearly visible.

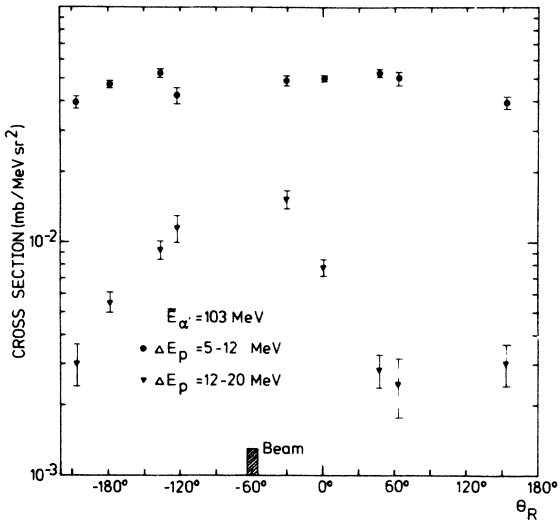

FIG. 5. As for Fig. 4, but for $\bar{E}_{\alpha'} = 103$ MeV.

channels were not present except for very small momentum transfers. This may be seen from a Dalitz plot for a coplanar geometry (Fig. 3). It can be seen that most chance coincidences were registered with elastically scattered α particles, which have not been subtracted for this figure. The density of points is largest for the evaporation band around 5 MeV. The ground state corresponding to the reaction ^{58}Ni$(\alpha,\alpha' p_0)^{57}$Co is indicated as a solid curve.

To study the dependences of coincidence proton cross sections on α energies, detection angles, and proton energies, the data were first transformed into the rest system of the recoiling nucleus. Because of the finite sizes of the α'-energy bins, the transformation yields an uncertainty in the angle of approximately 10°, which is indicated in Figs. 4 and 5 as the uncertainty of the incident beam direction.

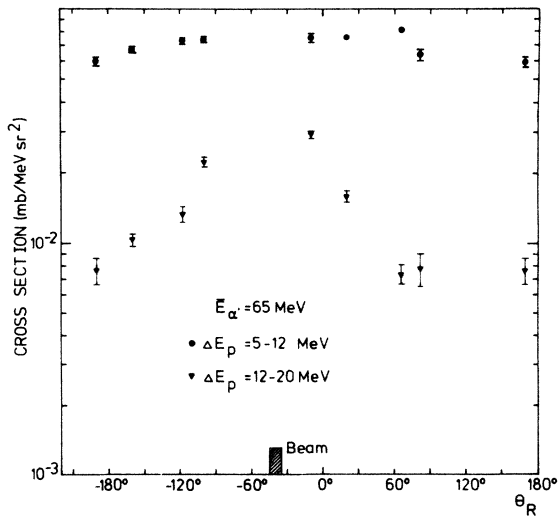

FIG. 4. Angular distributions of protons coincident with α' particles having a mean energy $\bar{E}_{\alpha'} = 65$ MeV. The different symbols represent two different proton energy bins. The data are presented in the rest system of the recoiling nucleus. Thus, the beam direction becomes uncertain, as discussed in the text.

The proton yields have been summed up for two nearly equally spaced bins: from 5 to 12 MeV, which corresponds to the evaporation region, and from 12 to 20 MeV. The angular distributions for two different α' energies are shown in Figs. 4 and 5. The angular behavior of both proton bins seems to be independent of the energy transfer. The low energy bin seems to be more or less isotropic while the higher energy bin indicates a strong anisotropy. While the first observation reminds one again of spectral shapes of an underlying evaporation process, a peaking into the beam direction seems to be surprising upon first view. For a one-step process, without considering the effect of distortions, a maximum in momentum transfer direction should be expected. This is not the case (see especially Fig. 5). However, neglecting the influences of distortions might be an oversimplification. The cross section for both proton energy bins increases with increas-

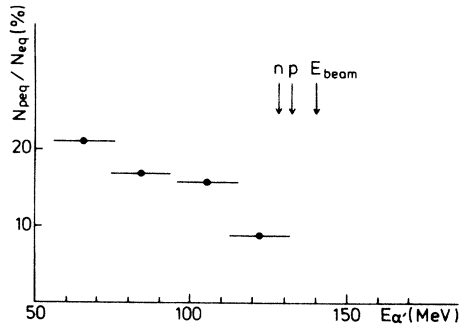

FIG. 6. Ratio of the total number of preequilibrium protons emitted in the energy interval 12 to 20 MeV to the total number of protons emitted in the equilibrated energy range 5–12 MeV as a function of the outgoing α' energy. The arrows indicate neutron and proton emission thresholds and the beam energy, respectively.

ing energy transfer. While the cross section is $\sim 7.5\times10^{-2}$ mb/MeV sr^2 for $\bar{E}_{\alpha'}=65$ MeV, it is $\sim 5\times10^{-2}$ mb/MeV sr^2 for $\bar{E}_{\alpha'}=103$ MeV. The increase is even more dramatic for the high energy bin corresponding to nonequilibrium protons. In Fig. 6 the ratio of the angle integrated yields for both proton energy bins is shown as a function of the α' energy. Obviously more and more yield goes in preequilibrium particle emission as the energy of the excited ^{58}Ni nucleus increases.

Now we want to discuss the $(\alpha,2\alpha)$ reactions. Compared to the $(\alpha,\alpha'\mathrm{p})$ reactions, the counting rate statistics is rather poor. This can be seen from the error bars shown in Fig. 7, where both reactions are depicted for an energy $\bar{E}_{\alpha'}=84$ MeV. Shown are the differential multiplicities, which are defined as the ratio of coincident to singles cross section

$$\frac{dM_c}{d\Omega_c}=\int_{\epsilon_1}^{\epsilon_2}\frac{d^4\sigma_{\alpha',c}}{d\epsilon_c d\Omega_c dE_{\alpha'}d\Omega_{\alpha'}}\Big/\frac{d^2\sigma_{\alpha'}}{dE_{\alpha'}d\Omega_{\alpha'}}d\epsilon_c\ , \quad (1)$$

as a function of the detection angle of the particle c. Although for $c=\mathrm{p}$ the detection range (5 to 20 MeV) and therefore the integration range in Eq. (1) is rather small when compared to the case $c=\alpha$ (8 to 78 MeV), the corresponding multiplicities are rather large. Since for proton emission evaporation is the dominating process (see Fig. 6), the differential multiplicities show the associated angular behavior: the differential multiplicity $dM_\mathrm{p}/d\Omega_\mathrm{p}$ is more or less isotropic. In contrast to that, $dM_\alpha/d\Omega_\alpha$ is strongly anisotropic and seems to peak somewhere between the beam and the recoil direction. This is even more true for the cases with smaller energy and momentum transfer than for the case shown in Fig. 7. This difference as compared to the nonequilibrium protons may be attributed to the contributions of knockout α particles. In Fig. 8 the spectra of the deep inelastically scattered α particles are shown for different detection angles of the particle $c=\alpha$. The spectra are rather flat and structureless except for 30° and 60°. These two angles are close to the direction of the transferred momentum. We will in the following concentrate on these two angles. In Fig. 9 we show spectra for $c=\alpha$ particles for the two angles which are closest to the recoil direction. The mean energy of the α' bin is indicated in the figures. The arrows show the kinematical limits for quasifree processes, i.e., smallest momentum transfer to the recoilng nucleus. For the lowest α' energy the quasifree region coincides with the evaporation region. In the other data shown—except for $\bar{E}_\alpha=65$ MeV and $\theta_\alpha=60°$—a knockout contribution is visible.

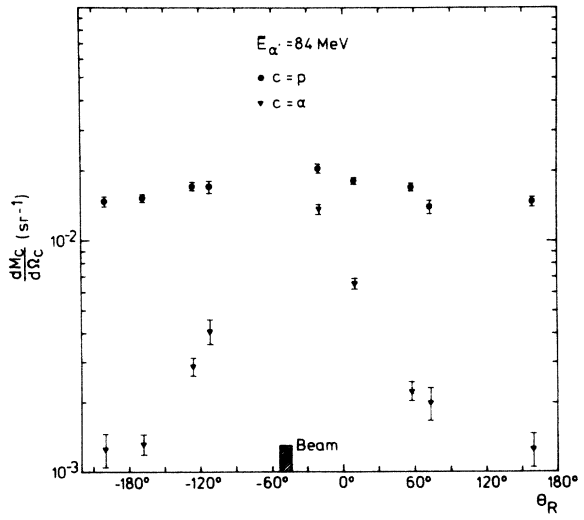

FIG. 7. Comparison of the differential p and α multiplicities in the rest system of the recoiled nucleus at $\bar{E}_{\alpha'}=84$ MeV. Proton spectra are integrated from 5 to 20 MeV, α spectra from 8 to 78 MeV.

IV. COMPARISONS WITH MODELS

Since most of the present models for describing continuous particle spectra have been recently reviewed, as discussed in the Introduction,[1] we will concentrate here on specific details of the models.

A. Estimates of involved times

One model which recently attracted much interest is the concept of local equilibrium.[4,13] It was originally introduced by Bethe[14] in qualitative form only and later put forward by the Marburg group (see Ref. 4 for a review). In order to detect spot heating in a nuclear reaction, the following relations between different times must hold:

$$\tau_c \le \tau_d \le \tau_s\ . \quad (2)$$

Here τ_c denotes the time to build up a local equilibrated system, τ_d denotes its decay time, and τ_s denotes the time necessary to spread the heat over the whole nucleus. To derive time estimates we will concentrate on the $\alpha+^{58}$Ni system. It was pointed out[15] that for hard spheres only two to three collisions per sphere are necessary to establish an almost equilibrium momentum distribution. In the exciton coalescence model[16–18] the deep inelastic α scattering is treated as if the incident α particle dissolves in the nuclear potential well into four nucleons. Thus, after one interaction the initial state is characterized by $n_0=5$ particles + 1 hole. After four residual interactions the angular distribution of a fast particle is almost isotropic. For the chosen reaction ^{58}Ni+α at 35 MeV/nucleon the time to reach an 8p + 4h state is 1.4×10^{-22} s, as estimated from the solution of the master equation. However, the time to reach thermal equilibrium is not much longer: 2.2×10^{-22} s.

The decay time τ_d can be estimated by integration over the emission rate, leading for neutron emission to[19]

$$\tau_d=\frac{\pi\hbar^3}{(2s+1)R^2\mu T^2(U-B)}e^{B/T(U)}\ . \quad (3)$$

In this equation the nuclear radius is denoted by R, the reduced mass by μ, and the ejectile spin by s. The excitation energy is denoted by U and the binding energy by B. Equation (3) is plotted versus the temperature $T(U)$ in

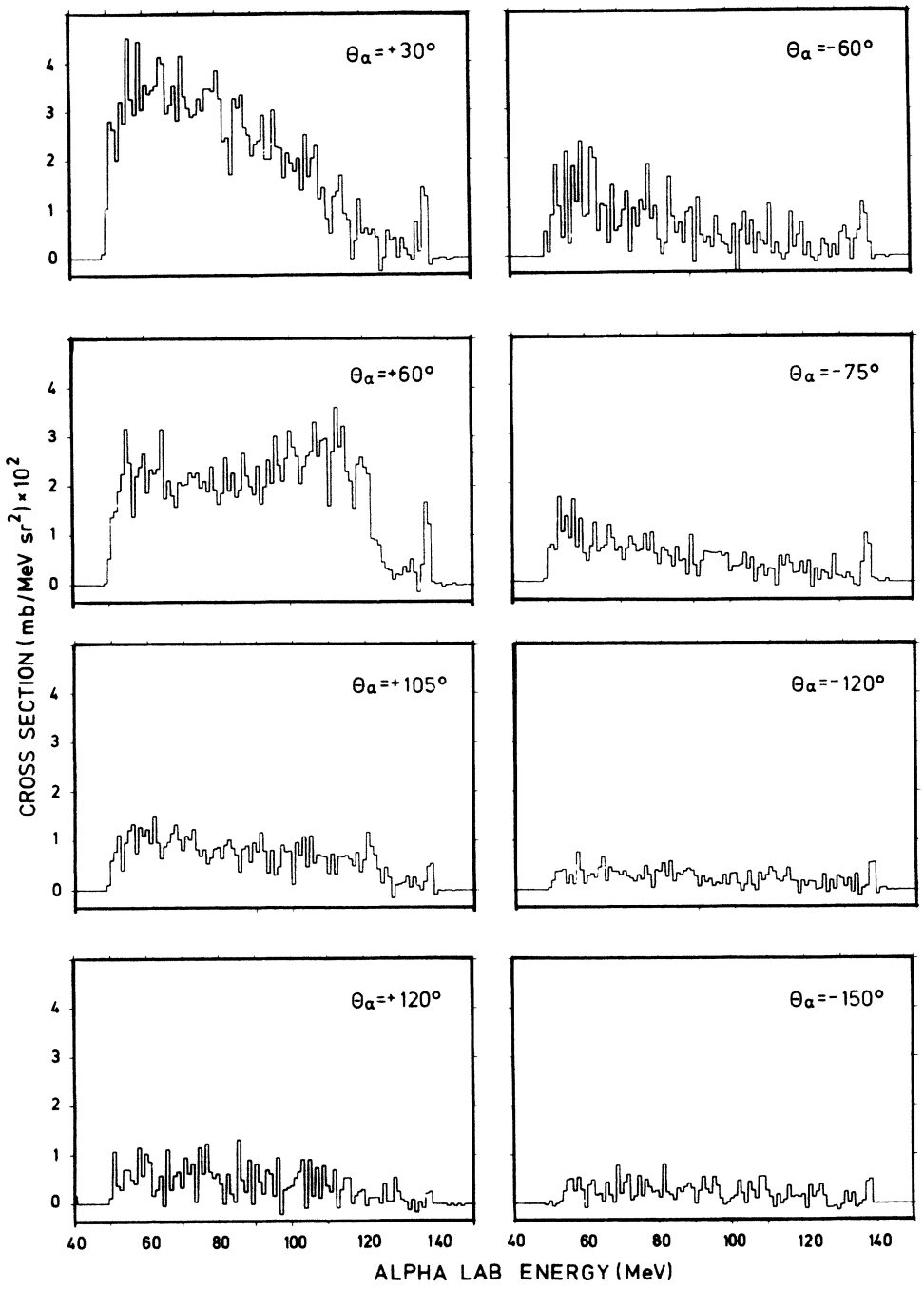

FIG. 8. Spectra of α particles scattered to $\vartheta_{\alpha'} = -30°$ in coincidence with α particles having energies between 8 and 78 MeV at detection angles indicated in the figure.

Fig. 10. The excitation energy has been calculated from the Fermi gas equation of state

$$U = aT^2 , \tag{4}$$

with $a = N/8$ MeV^{-1} and N the number of nucleons sharing the energy. A typical binding energy of $B = 10$ MeV was assumed. Surprisingly, the decay time depends only weakly on N for temperatures above 3 MeV.

The spreading time may be estimated according to Tomonaga.[20] He derived a formula for the half-life that in infinite nuclear matter with temperature 0 in one half and temperature T in the other half, the temperature will change by $T/4$ at a distance R from the origin. The result is

$$\tau_s = \frac{1}{0.92} \frac{m\rho c R^2}{K} , \tag{5}$$

with c the specific heat, ρ the density, K the heat conduc-

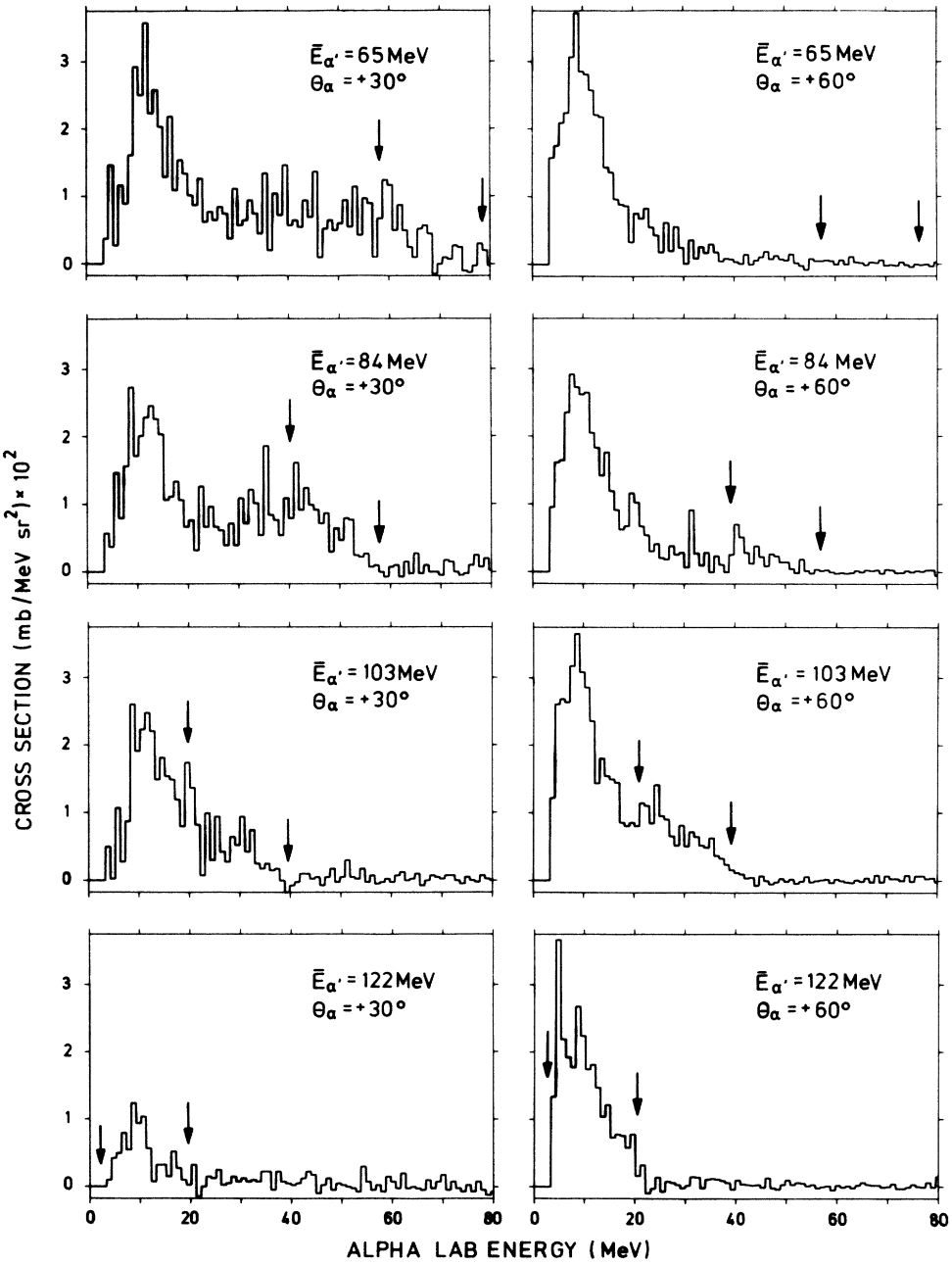

FIG. 9. Spectra of $c=\alpha$ particles detected at $\theta_\alpha=30°$ (left-hand side) and $\theta_\alpha=60°$ (right-hand side) in coincidence with α' particles detected at $\vartheta_{\alpha'}=-30°$ and mean energies $\bar{E}_{\alpha'}$ indicated in the figure. The arrows indicate the interval with the smallest recoil momentum.

tivity of nuclear matter, and m the nucleon mass. Inserting specific heat and heat conductivity equations for a Fermi gas into Eq. (5) yields[21]

$$\tau_s = 163.4 \frac{R^2\sqrt{m}}{\epsilon_F^{5/2}} \frac{T^2}{\Lambda(\epsilon,T)} . \quad (6)$$

The mean free path Λ depends on the energy of the nucleon under consideration and the temperature of its surroundings. The most probable energy in a Maxwellian distributed source is $2T$. If we assume a temperature of $T/2$ at the surface between the cold and hot pieces on the average the kinetic energy is $\epsilon=\epsilon_F+T$ which, at the temperatures under discussion here, is mainly the Fermi energy ϵ_F. It should be mentioned that the mean free path values entering the calculations are for $T=0$ the same as the ones used in the exciton coalescence model calculations, i.e., assuming the reaction taking place—averaged over all impact parameters—at a density ρ which is half the nuclear matter saturation density. Equation (6) is also shown in Fig. 10. Obviously, for temperatures exceeding 3 MeV the relation $\tau_s \geq \tau_d$ holds. However, only in a region around 3.5 MeV is relation (2) valid.

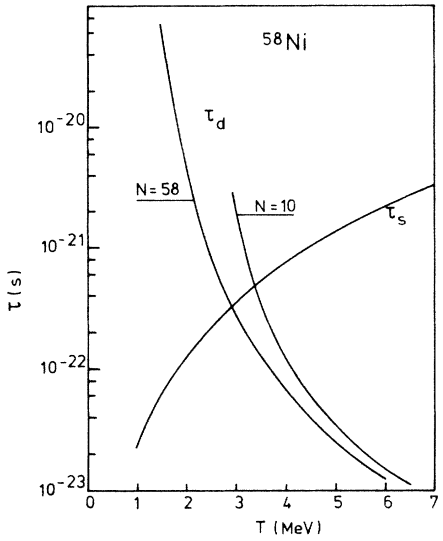

FIG. 10. The dependence of the spreading time τ_s and the decay time τ_d as a function of the temperature T. The decay time is shown for the fully equilibrated ($N=58$) compound nucleus and for a subsystem consisting of $N=10$ nucleons.

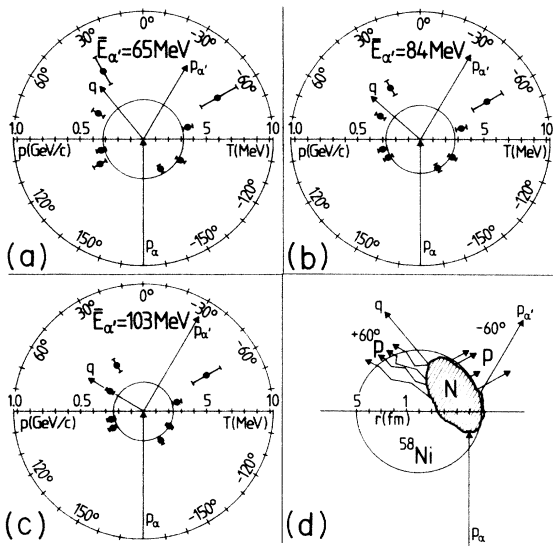

FIG. 11. Angular dependence of the extracted local temperaturelike parameter T for $\overline{E}_{\alpha'}=65$ MeV [part (a)], $\overline{E}_{\alpha'}=84$ MeV [part (b)], and $\overline{E}_{\alpha'}=103$ MeV [part (c)]. The linear momenta of the incoming and outgoing α particles (p_α and $p_{\alpha'}$, respectively) as well as the momentum transfer q are indicated by arrows. The small circle indicates the temperature of the fully equilibrated system at corresponding energy transfers. (d) Schematic picture of the underlying reaction mechanism (see the text). The shaded area indicates the early stage of the equilibration process.

In the time τ_c four interactions have already taken place which have exhausted nearly all the preequilibrium yield. Here preequilibrium means all processes leading to excitations of states in the continuum. One can therefore expect to see fingerprints of a spot heating not in the high energy part of the spectra but only in the low energy part.

B. Data analysis in terms of local equilibrium

As pointed out above, spot heating may be visible only in the evaporative region. Since we do not know whether emission from a hot spot is a surface or volume effect, the preexponential factor[22] in a Maxwell-Boltzmann distribution is unknown. We therefore have fitted an exponential $e^{-\epsilon/T}$ to the proton cross sections in a region from 5 to 12 MeV. Surprisingly, the extracted slope parameters show an angle dependence which is shown in Fig. 11 for three different $\overline{E}_{\alpha'}$ values. The momenta involved are also indicated in the figure. While at backward angles the T parameters are in agreement with the assumption of emission from a fully equilibrated system—the compound nucleus temperature is shown as a circle—the values obtained at forward angles are larger. In a very schematic model we can assume the momentum and energy brought into the system by the scattered α particle to be distributed on a group of nucleons. From energy and momentum conservation together with Eq. (4) we obtain nucleon numbers from 7 to the fully equilibrated system depending on energy transfer and angle of observation. The numbers are listed in Table II. If the group of nucleons is confined in coordinate space and moves through the nucleus while it decays by particle emission or by heating up the remaining system as indicated in Fig. 11(d), the behavior of the T parameter may be understandable. Such a model[11] reminds one of the drifting hot spot model independently formulated.[23]

Fitting of just an exponential seems not to be adequate in terms of such a model. If we suppose a Maxwell-Boltzmann distribution in the rest system of the heated nucleon group, transformation into the laboratory system yields

$$\sigma = c\sqrt{\epsilon}\exp\{-[\epsilon-\sqrt{2u\epsilon}v_s\cos(\theta_R-\theta_p)+\tfrac{1}{2}mv_s^2]/T\}\ , \tag{7}$$

with u denoting the nucleon mass and the v_s the mean velocity of the nucleon group. The angle is calculated relative to the direction of momentum transfer or the recoil direction θ_R. The T parameters obtained by fitting Eq.

TABLE II. Number of nucleons sharing the excitation energy U as estimated from the slope parameter T.

θ_{lab}	$\overline{E}_{\alpha'}=65$ MeV	$\overline{E}_{\alpha'}=84$ MeV	$\overline{E}_{\alpha'}=103$ MeV
−150°	71^{+17}_{-12}	57^{+14}_{-10}	35^{+10}_{-7}
−120°	49^{+14}_{-10}	49^{+14}_{-10}	49^{+11}_{-8}
−75°	41^{+12}_{-8}	37^{+11}_{-7}	37^{+8}_{-6}
−60°	11^{+9}_{-4}	10^{+8}_{-4}	7^{+6}_{-7}
+ 30°	13^{+8}_{-4}	18^{+6}_{-5}	14^{+6}_{-4}
+ 60°	32^{+10}_{-7}	29^{+9}_{-6}	29^{+7}_{-6}
+ 105°	46^{+12}_{-8}	41^{+10}_{-7}	39^{+8}_{-7}
+ 120°	34^{+11}_{-8}	46^{+12}_{-8}	35^{+8}_{-6}

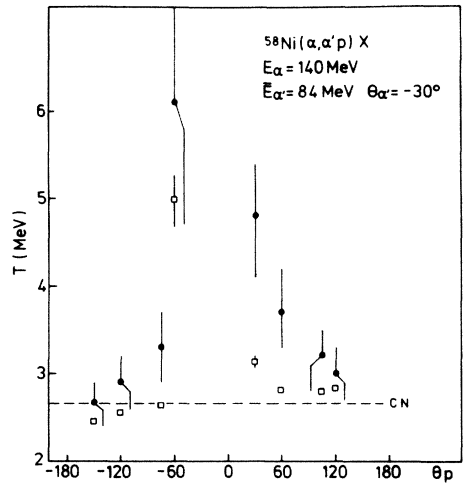

FIG. 12. Extracted slope parameters T of the coincident proton yields for energies from 5 to 12 MeV. Fits with only exponentials [compare with Fig. 11(b)] are represented by dots, those with Eq. (7) are shown as squares. The temperature of a fully equilibrated system is indicated as a dashed line.

(7) to the data show the same behavior as those obtained by fitting only exponentials. An example is given in Fig. 12 for the energy bin with $\bar{E}_{\alpha'}=84$ MeV. For this case the source velocity is $v_s \sim 0.02c$. From only momentum conservation the number of nucleons in the source is found to be approximately 26. However, momentum and energy conservation are not achievable at the same time with respect to the fitted quantities. A large source size may reflect this deficiency of the analysis. A way out might be the assumption of energy and momentum going into rotation. It should be noted that the same results are obtained when the acceleration of the protons in the Coulomb field is taken into account in Eq. (7). One could argue that the high temperatures obtained at $\vartheta_p=+30°$ and $-60°$ were simulated by the nonevaporative component which is not explicitly accounted for in the low energy interval. We have therefore fitted two exponentials to the whole range of energies, i.e., 6 to 20 MeV. Again the two angles mentioned above indicate larger slope parameters than obtained for the other angles. As an example, the values for the bin with $\bar{E}_{\alpha'}=84$ MeV are $T=3.29\pm0.11$ MeV and 4.47 ± 1.04 MeV for 30° and $-60°$, respectively. These values are larger than the compound nucleus temperature indicated in Figs. 11(b) and 12, even when the error (on a 66% confidence level) is taken into account. Because of small coincidence cross sections, especially at $\vartheta_p=-60°$, the deduced temperatures indicate large uncertainties. Therefore, comparisons with the present data cannot be made including error bars of two to three standard deviations. The other angle data yield $T \lesssim 3$ MeV. In addition, the multiplicity of the low energy component at $\vartheta_p=-60°$ is the smallest one. This finding supports the assumed reaction mechanism sketched in Fig. 11(d).

C. Exciton coalescence model calculation

We now turn to the high-energy nonevaporative part of the proton spectra and try to understand this part in terms of a multistep process. The exciton coalescence model mentioned above was originally developed to reproduce inclusive spectra of fast secondary particles.[16,17] Recently it was shown that coincident particle emission may also be described within this model.[18] The starting point for the process is the assumption that a projectile nucleon interacts with a target nucleon leading to a state characterized by an excitation of five particles and one hole with respect to the Fermi surface. The equilibrium process leads then to more complex excitations. In any state an α particle or a nucleon or both may be emitted. Thus both emission processes are to a large extent statistically independent and not separated in time. The equilibration process is described by a system of master equations for each system under consideration. It is further assumed that after any residual interaction the scattered and the struck nucleon carry memory of the incident direction. The direction of the fast particles is calculated under the assumption that both particles undergo the same linear momentum dissipation process. In Fig. 13 the inclusive α' cross sections are shown together with the exciton coalescence model result. The absolute height of the calculation was obtained by fitting the coalescence radius P_0 to the data. Within the model α-particle formation occurs when two neutrons and the protons have momenta confined within a sphere in momentum space with radius P_0. This is the only individually adjusted model parameter. The coincidence proton yields for two α'-energy bins are shown in Figs. 14 and 15 together with model predictions. For the reaction with small energy transfer the yields are dominated by evaporative processes, except for the forward angles. In the case of a large energy transfer the high energy part is for all angles dominated by the preequilibrium cross section.

D. Quasifree processes

There is evidence[24,25] that quasifree scattering is the doorway state to multistep processes like those described by the exciton coalescence model. Even the whole equilibration cascade has been treated as a series of quasifree

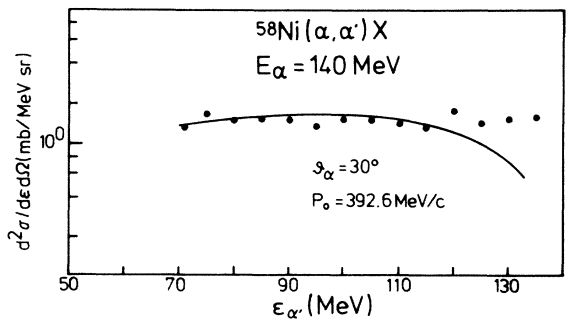

FIG. 13. Inclusive yields for the indicated reaction. The data are shown as dots and the exciton coalescence model calculation as a solid line. The coalescence radius P_0 obtained by normalizing the calculation to the data is indicated.

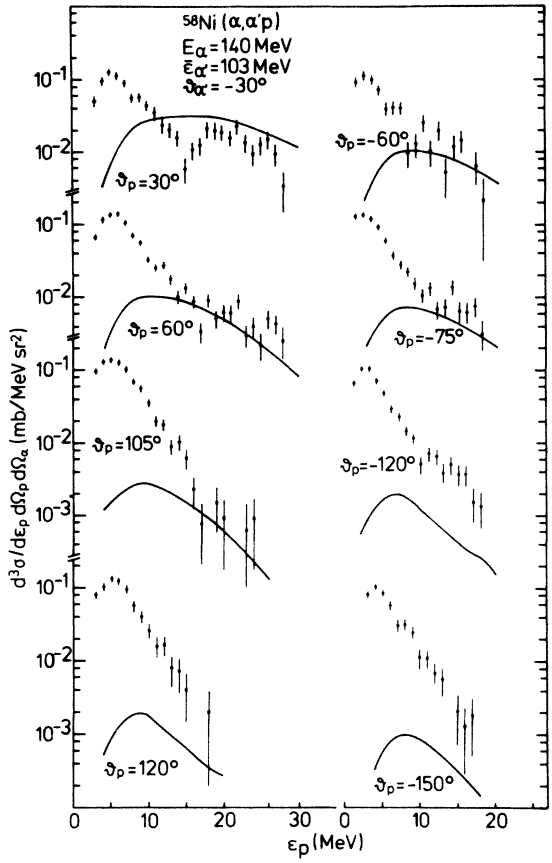

FIG. 14. Coincident proton cross sections are compared with exciton coalescence predictions. The mean α' energy is $\bar{E}_{\alpha'}=103$ MeV.

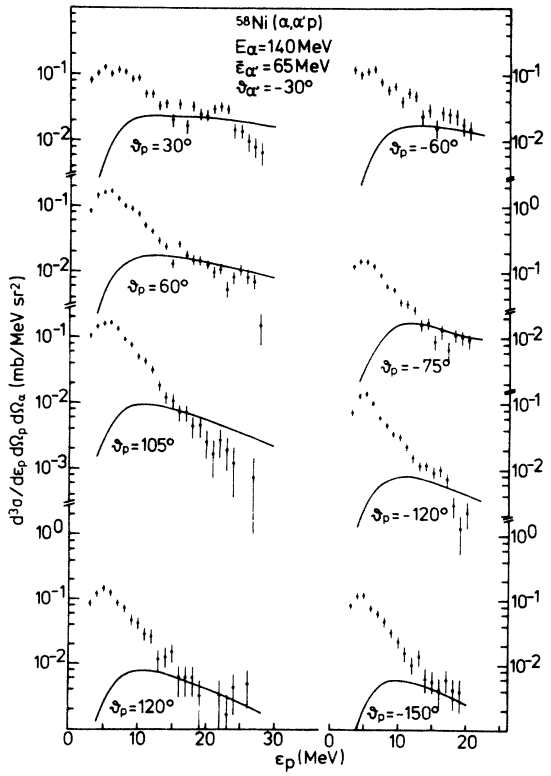

FIG. 15. As for Fig. 14, but for $\bar{E}_{\alpha'}=65$ MeV.

scattering processes.[26] Inspired by such models we can assume that the incident α particle hits a target nucleon which then initiates an equilibration cascade. We then could expect the coincident proton spectra for the different energy transfers to have shapes like those from inclusive (p,p') reactions at the same excitation energy. We have therefore compared our coincident spectra with ^{54}Fe(p,p') data[27] for $\vartheta_{p'}=|\theta_R-\theta_p|$. The absolute height was suitably normalized to our data. The corresponding results are shown in Figs. 16–18 for the different energy transfers. While for coincident proton emission to the same side as α' emission, i.e., negative angles in our convention, the inclusive data follow the shape of the coincidence data, there is strong disagreement between both for positive angles. If we plot just the same laboratory angles on top of each other and neglect the recoil direction, we find a rather satisfactory agreement between inclusive and coincident data. The normalization factors employed were distributed around $(9.0\pm0.5)\times10^{-3}$ sr^{-1}, $(8.1\pm0.5)\times10^{-3}$ sr^{-1}, and $(7.9\pm0.5)\times10^{-3}$ sr^{-1} for the bins having a mean α' energy of 65, 84, and 103 MeV, respectively. This can be understood if the two emission processes of the α' particle and the proton are statistically independent, as is assumed in the exciton coalescence model. We can therefore conclude that the $(\alpha,\alpha'p)$ reaction with ejectile energies covered in our experiment is not of single-step nature.

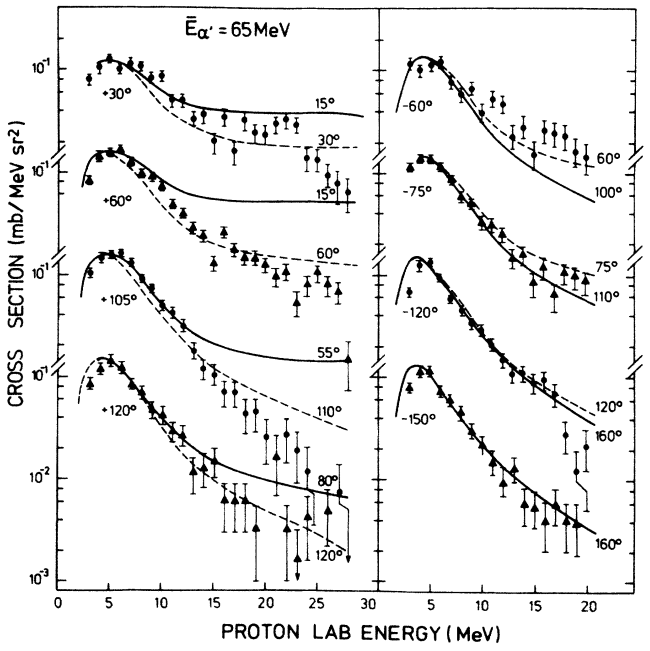

FIG. 16. Coincident proton cross sections (data points) are compared with inclusive ^{54}Fe(p,p')X cross sections (curves) normalized to the coincident ones. The proton energy $E_p=62$ MeV leads to an excitation energy close to 75 MeV achieved with $\bar{E}_{\alpha'}=65$ MeV. The observation angles of the coincident data θ_p are written on the left-hand side, those for the inclusive data on the right-hand side. The solid curves correspond to $\vartheta_{p'}=|\theta_R-\theta_p|$ (rest system of the recoiling nucleus) and the dashed curves correspond to $\vartheta_{p'}=|\theta_p|$ (laboratory system).

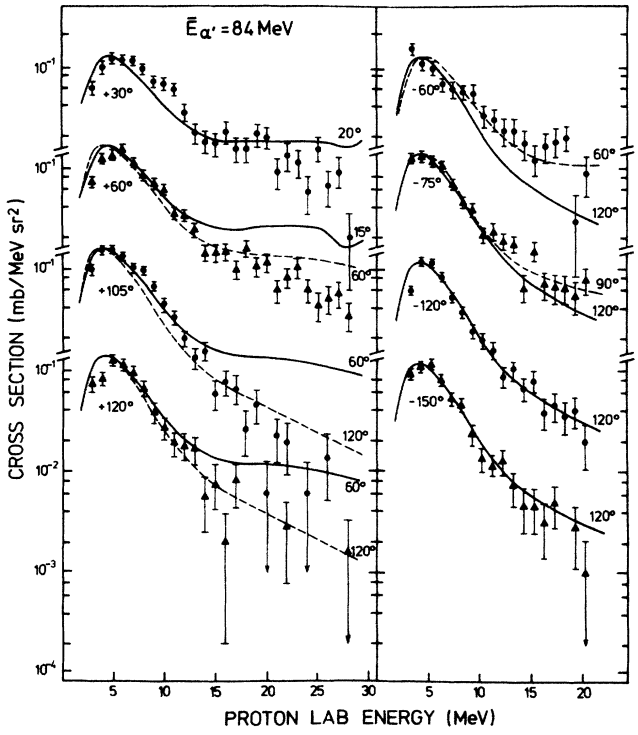

FIG. 17. As for Fig. 16, but for $E_p = 39$ MeV and $\bar{E}_{\alpha'} = 84$ MeV.

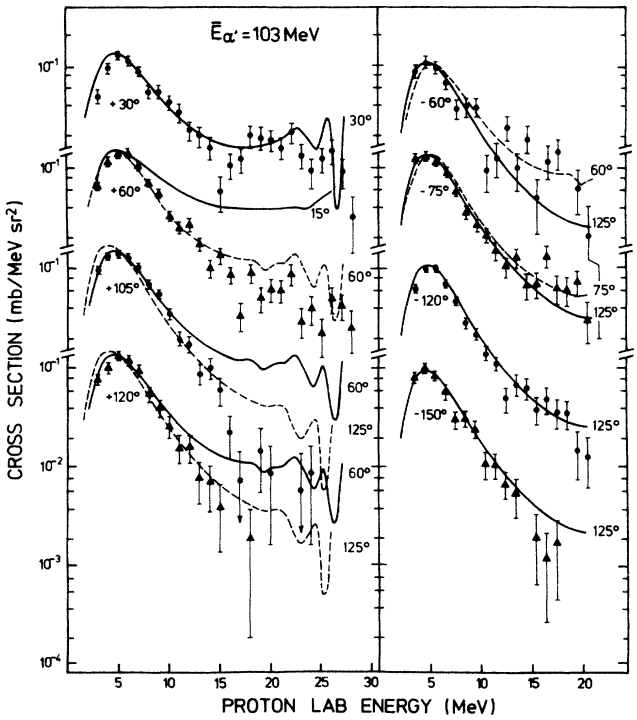

FIG. 18. As for Fig. 16, but for $E_p = 29$ MeV and $\bar{E}_{\alpha'} = 103$ MeV.

This finding seems to contradict the results of Ref. 28, where ^{58}Ni(p,2p) reactions at $E_p = 200$ MeV were reported. The direction of the struck nucleon has been calculated in a quasifree approximation using distorted waves for the incident and scattered proton and plane waves for the struck proton. There, inclusive (p,p') cross sections reproduce the data under the assumption that the struck proton starts the equilibration cascade. The mean angle for the struck nucleon differs markedly from the direction of momentum transfer, which is simply assumed in our comparison as the direction of the struck nucleon. Only if distortions will in the case of the $(\alpha,\alpha'p)$ reaction lead to a mean direction of the struck proton momentum distribution close to the beam direction are our results not in contradiction with the quasifree scattering assumption. However, this seems not to be the case, as can be seen from the $(\alpha,\alpha_1\alpha_2)$ measurements. If we again assume the emission of the two α particles to be statistically independent, then we can compare the $(\alpha,2\alpha)$ data with inclusive (p,α) data. Such a comparison is made in Fig. 19 for $\bar{E}_{\alpha_1} = 84$ MeV with ^{54}Fe(p,α) data[27] for the same laboratory angles as for the α_2 particles. Again the inclusive data are suitably normalized to our $(\alpha,2\alpha)$ data with normalization factors of $(1.5\pm0.3)\times10^{-2}$ sr^{-1}. The inclusive data show the same spectral shapes as the coincidence

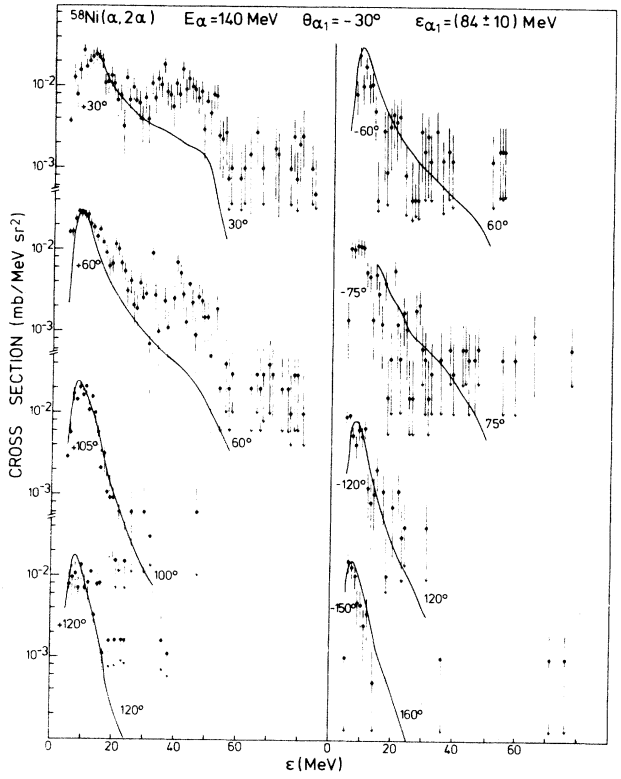

FIG. 19. Coincident α-particle cross sections for the mean α' energy $\bar{E}_{\alpha'} = 84$ MeV are compared with the inclusive ^{54}Fe(p,α)X yield at $E_p = 62$ MeV normalized to the coincident data. The laboratory angles for the coincident particles are indicated on the left-hand side, those for the inclusive reaction on the right-hand side.

data except for the two angles $\theta_{\alpha_2} = +30°$ and 60°, which are the two angles closest to the direction of momentum transfer. In these two spectra bumps from quasifree $(\alpha,2\alpha)$ scattering show up. We take this as evidence that even with distortions the direction of the struck nucleon is close to the direction of momentum transfer.

Another difference between the (p,2p) reaction and the $(\alpha,\alpha'p)$ reaction, which makes a direct comparison between them not easy, is the mean free path of the projectile particle. According to the optical model estimate

$$\Lambda = \frac{\hbar v}{2W} , \tag{8}$$

we get $\Lambda_p \sim 6.5$ fm from the optical model parameters obtained in Ref. 29 and $\Lambda_\alpha \sim 1.8$ fm from those in Ref. 30 for the nucleus ^{58}Ni. Because of the longer mean free path, the scattered protons have a greater chance to emerge before suffering another collision than the α particles have. This leads to a stronger localization of the α interactions than of proton interactions. Another aspect of the different mean free paths is that the α particles probe only the outer regions of the nucleus while the protons probe more dense regions. Therefore, in the (p,2p) reactions it was assumed[28] that the second proton is struck from $2s_{1/2}$ and $1f_{7/2}$ orbitals. The mean angle was obtained including the distortions by the incoherent sum of both contributions. In the α-induced reaction we can assume an interaction with protons from the $1f_{7/2}$ orbital. Why contributions of the $1d_{3/2}$ orbitals have been neglected in Ref. 28 is unclear to us.

V. CONCLUSIONS

In summary, we have measured deep inelastic scattered α particles in coincidence with other charged particles emitted into the reaction plane. The particles measured were nearly all protons and α particles. The number of emitted protons greatly exceeds the number of emitted α particles (cf. Fig. 7). This is not the case in heavy-ion-induced reactions.[31] In the reaction ^{58}Ni + 96 MeV ^{16}O the number of neutrons measured in coincidence with deep inelastically scattered projectile particles is close to the number of α particles.[31,32] This fact sheds light on possible different reaction mechanisms mainly with respect to the angular momenta involved. Differences with respect to investigations with 200 MeV incident protons were discussed in the preceding section.

The coincident proton spectra show in the evaporation region T parameters which depend on the detection angle. These T parameters exceed compound nucleus values at forward angles. We have proposed a simple model describing this behavior in terms of an equilibration process where an almost statistical source moves through the nucleus and loses its energy density by heating the surrounding nucleus and by particle emission.

Results of the present investigation indicate the presence of various processes contributing to the deep inelastic scattering of alpha particles of energies higher than 100 MeV on medium weight nuclei. We have proved the existence of the preequilibrium emission of coincident particles uncorrelated with the four-momentum transfer as well as measurable contribution of quasifree scattering from alpha clusters. It was found that the preequilibrium emission of coincident ejectiles can be well accounted for by the exciton coalescence model.[18] More experiments of the exclusive type extending to smaller α scattering angles, higher ejected proton energies, and possibly including neutron spectra, too, are required to get a full picture of the mechanism of deep inelastic scattering of alpha particles.

---

*Permanent address: Institute of Nuclear Physics, Cracow, Poland.

[1]H. Machner, Phys. Rep. **127**, 309 (1985), and references therein.

[2]J. P. Bondorf, J. N. De, A. O. T. Karvinen, G. Fai, and B. Jokobsson, Phys. Lett. **84B**, 162 (1979).

[3]K. T. R. Davies, B. Remaud, M. Strayer, K. R. Sandy Devi, and Y. Raffray, Ann. Phys. (N.Y.) **156**, 68 (1984).

[4]N. Stelte and R. Weiner, submitted to Rev. Mod. Phys., and references therein.

[5]C. K. Gelbke, in *Proceedings of the Workshop on Coincident Particle Emission from Continuum States in Nuclei, Bad Honnef, 1984*, edited by H. Machner and P. Jahn (World-Scientific, Singapore, 1984), p. 230.

[6]B. Sinha, Phys. Rev. Lett. **50**, 91 (1983).

[7]R. P. Schmitt, G. J. Wozniak, G. U. Rattazizi, G. J. Mathews, R. Regimbart, and L. G. Moretto, Phys. Rev. Lett. **46**, 522 (1981).

[8]A. Kiss, C. Mayer-Böricke, M. Rogge, P. Turek, and S. Wiktor, Phys. Rev. Lett. **33**, 1188 (1976).

[9]D. R. Brown, J. M. Moss, C. M. Rozsa, P. H. Youngblood, and J. D. Bronson, Nucl. Phys. **A313**, 157 (1979).

[10]A. Gamp, J. C. Jacmart, N. Poffé, H. Doubre, J. C. Roynette, and J. Wilczinski, Phys. Lett. **74B**, 215 (1978).

[11]U. Bechstedt, H. Machner, A. Budzanowski, P. Jahn, and C. Mayer-Böricke, Phys. Rev. C **25**, 3221 (1982).

[12]U. Bechstedt, Ph.D. thesis, Universität Bonn, 1982, Jülich Report Jül-1797, 1982.

[13]*Proceedings of the Workshop on Local Equilibrium in Strong Interaction Physics, Bad Honnef, 1984*, edited by D. K. Scott and R. M. Weiner (World-Scientific, Singapore, 1985).

[14]H. A. Bethe, Phys. Rev. **53**, 675 (1938).

[15]B. J. Alder and T. Wainwright, in *Transport Processes in Statistical Mechanics*, edited by I. Progogine (Interscience, New York, 1958), p. 97.

[16]H. Machner, Phys. Lett. **86B**, 129 (1979).

[17]H. Machner, U. Bechstedt, A. Djaloeis, and P. Jahn, Phys. Rev. C **26**, 411 (1982).

[18]H. Machner, Phys. Rev. C **29**, 109 (1984).

[19]V. F. Weisskopf, Phys. Rev. **52**, 295 (1937).

[20]S. Tomonaga, Z. Phys. **110**, 573 (1938).

[21]H. Machner, Z. Phys. A **316**, 201 (1984).

[22]A. S. Goldhaber, Phys. Rev. C **17**, 2243 (1978).

[23]N. Stelte, M. Weström, and R. M. Weiner, Nucl. Phys. **A384**,

190 (1982).
[24]A. M. Kalend, B. D. Anderson, A. R. Baldwin, R. Madey, J. W. Watson, C. C. Chang, H. D. Holmgren, R. W. Koontz, J. R. Wu, and H. Machner, Phys. Rev. C **28**, 105 (1983).
[25]H. Machner, D. Protić, G. Riepe, J. P. Didelez, N. Frascaria, E. Gerlic, E. Hourani, and M. Morlet, Phys. Lett. **138B**, 39 (1984).
[26]A. Mignerey, M. Blann, and W. Scobel, Nucl. Phys. **A273**, 125 (1976).
[27]F. E. Bertrand and R. W. Peelle, Phys. Rev. C **8**, 1045 (1973).
[28]C. Ciangaru, C. C. Chang, H. D. Holmgren, A. Nadasen, P. G. Roos, A. A. Cowley, S. Mills, P. P. Singh, M. K. Saber, and J. R. Hall, Phys. Rev. C **27**, 1360 (1983).
[29]A. Nadasen, P. Schwandt, P. P. Singh, W. W. Jacobs, A. D. Baeker, P. T. Debevec, M. D. Kaitchuck, and J. T. Meek, Phys. Rev. C **23**, 1023 (1981).
[30]D. A. Goldberg, S. M. Smith, and G. F. Burdzik, Phys. Rev. C **10**, 1362 (1979).
[31]H. Ho, R. Albrecht, W. Dünnweber, G. Graw, S. G. Steadman, J. P. Wurm, D. Disdier, V. Rauch, and F. Schiebling, Z. Phys. A **283**, 235 (1977).
[32]H. Gemmeke, P. Netter, Ax. Richter, L. Lassen, S. Lewandowski, W. Lücking, and R. Schreck, Phys. Lett. **97B**, 213 (1980).